Vertebral trabecular bone texture analysis in opportunistic MRI and CT scan can distinguish patients with and without osteoporotic vertebral fracture: A preliminary study

François Poullain, Pierre Champsaur, Vanessa Pauly, Paul Knoepflin, Thomas Le Corroller, Maud Creze, Martine Pithioux, David Bendahan, Daphne Guenoun

Research article

Vertebral trabecular bone texture analysis in opportunistic MRI and CT scan can distinguish patients with and without osteoporotic vertebral fracture: A preliminary study

François Poullain [a], Pierre Champsaur [a,b], Vanessa Pauly [c,d], Paul Knoepflin [a], Thomas Le Corroller [a,b], Maud Creze [e], Martine Pithioux [b], David Bendahan [f], Daphne Guenoun [a,b,*]

[a] *APHM, Sainte-Marguerite Hospital, Institute for Locomotion, Department of Radiology, 13009 Marseille, France*
[b] *Aix Marseille Univ, CNRS, ISM, Inst Movement Sci, Marseille, France*
[c] *Aix Marseille Univ, Unité de recherche EA3279, Santé Publique et Maladies Chroniques: Qualité de vie concepts, usages et limites, déterminants, 13005 Marseille, France*
[d] *APHM, Service de Santé Publique et d'Information Médicale, Hôpital de la Conception, Marseille, France*
[e] *Radiology Department, Bicêtre Hospital, APHP, Le Kremlin–Bicêtre, France*
[f] *Aix Marseille Univ, CNRS, CRMBM UMR 7339, 13385 Marseille, France*

ARTICLE INFO

Keywords:
Spine
Osteoporosis
Opportunistic
CT
MRI
Texture

ABSTRACT

Purpose: To investigate the potential of texture parameters from opportunistic MRI and CT for the detection of patients with vertebral fragility fracture, to design a decision tree and to compute a Random Forest analysis for the prediction of fracture risk.

Methods: One hundred and eighty vertebrae of sixty patients with at least one (30) or without (30) a fragility fracture were retrospectively assessed. Patients had a DXA, an MRI and a CT scan from the three first lumbar vertebrae. Vertebrae texture analysis was performed in routine abdominal or lumbar CT and lumbar MRI using 1st and 2nd order texture parameters. Hounsfield Unit Bone density (HU BD) was also measured on CT-scan images.

Results: Twelve texture parameters, Z-score and HU BD were significantly different between the two groups whereas T score and BMD were not. The inter observer reproducibility was good to excellent. Decision tree showed that age and HU BD were the most relevant factors to predict the fracture risk with a 93 % sensitivity and 56 % specificity. AUC was 0.91 in MRI and 0.92 in CT-scan using the Random Forest analysis. The corresponding sensitivity and specificity were 72 % and 93 % in MRI and 83 and 89 % in CT.

Conclusions: This study is the first to compare texture indices computed from opportunistic CT and MR images. Age and HU-BD together with selected texture parameters could be used to assess risk fracture. Machine learning algorithm can detect fracture risk in opportunistic CT and MR imaging and might be of high interest for the diagnosis of osteoporosis.

1. Introduction

Osteoporosis results from a combined alteration of bone density mineralization and bone trabeculae micro-structure and is related to an increased risk of fragility fractures [1]. In 2017, 2.7 million fragility fractures have been reported in Europe with almost twice as many fractures in women (66 %) as compared to men. Hip, vertebral and distal forearm fractures accounted for 19.6, 15.5 and 17.9 % of all fractures, respectively [1]. Vertebral fragility fractures lead to significant over-morbidity and mortality with severe back pain, height loss and kyphosis responsible for cardiovascular and respiratory disease [2].

Osteoporosis is most widely diagnosed on the basis of bone mineral density (BMD) measurements performed using dual-energy X-ray absorptiometry (DXA). However, it has been largely recognized that BMD alone is not a good predictor of fracture risk [3,4]. The corresponding T score which is based on a −2.5 standard deviation threshold has been

* Corresponding author APHM, Sainte-Marguerite Hospital, Institute for Locomotion, Department of Radiology, 13009 Marseille, France.
E-mail address: daphne.guenoun@ap-hm.fr (D. Guenoun).

criticized as a diagnostic index given that osteoporosis-related fractures can occur in patients with a normal DXA [3,4]. Despite the recognized limits of DXA, it is still the reference method for the diagnosis of osteoporosis.

Alternative methods targeting bone microarchitecture or images texture have been developed. For instance, Trabecular Bone Score (TBS) can be computed from DXA measurements but this index has been barely used for clinical applications. Yet, data regarding trabecular bone might be of interest [5]. Quantitative computed tomography (qCT) can be used to assess the 3D bone mineral density on conventional body scanner. Yet, for cost and irradiation reasons qCT is barely used [6]. Furthermore, it cannot provide additional information about bone texture or micro-architecture. Finite element analysis and biomechanical features have been used to improve the prediction of fracture risk but this type of approach is not usable in clinical routine [7].

Recently, mathematical algorithms have been growingly used in order to assess the inherent texture of biomedical images [8]. Texture analysis has been used to analyse the distribution and relationship of pixel or voxel grey levels within an image [9] and could be used for an opportunistic assessment of MRI and CT-scan images in osteoporosis [10].

In the field of lumbo-radicular pain, lumbar MRI is the reference method. While a large amount of patients with various pathologies are undergoing computed tomography (CT) of the lumbar spine, it could be of interest to use the corresponding images for an opportunistic osteoporosis screening. Given that dozens of parameters are provided by texture analysis, the challenge is to identify those of interest for a given application. If so, texture tool could be integrated into machine learning algorithms such as Random Forest analysis [11].

The main objective of the present study was to identify the texture parameters, if any, measured in opportunistic MRI and CT scans, and radiodensity measured in opportunistic CT scans that would be able to distinguish patients with and without a vertebral fragility fracture. The second objective was to propose a decision tree for the assessment of the fracture risk. The third objective was to perform a Random Forest analysis using this whole set of parameters and quantify the potential for fracture risk prediction.

2. Patients and methods

2.1. Patients

This retrospective study was approved by the local ethic committee (2019_120). Due to the retrospective nature of the study, the need for an informed consent was waived. As illustrated in Fig. 1, data were retrieved from our local database for patients who had DXA, lumbar MRI and thoraco-abdominal or lumbar CT between May 2018 and January 2020. DXA was available for at least 2 vertebrae among L1, L2, L3. CT scans were obtained without the use of intravenous contrast agent and had to cover entirely L1, L2 and L3. Lumbar MRI had at least a sagittal T1-weighted acquisition. The time between DXA, CT and MRI was no longer than 6 months.

Exclusion criteria were bone tumoral pathology (hematologic malignancies, solid tumor with bone metastasis, hemangioma, enostosis), high energy traumatism and low-quality exams (due to arthrodesis or cement in the lumbar spine).

Overall, sixty patients were included and divided in 2 groups regarding the presence or not of collapsed vertebrae, using the Genant semi-quantitative classification [12]. One or multiple osteoporotic vertebral fractures at the L1, L2 or L3 level was identified in thirty patients (Group 1: G1). The diagnosis of fractures was confirmed as a consensus between radiologists with an expertise ranging from 2 to 12 years (FP and DG). In the control group, the first thirty consecutive patients without vertebral fracture were selected to have the same number of patients in each group (Group 2: G2) (Fig. 1).

2.2. MRI acquisition and volume of interest (VOI)

Subjects were positioned supine, head first in the magnet bore with their lumbar region over the spine matrix coil. An MRI whole body

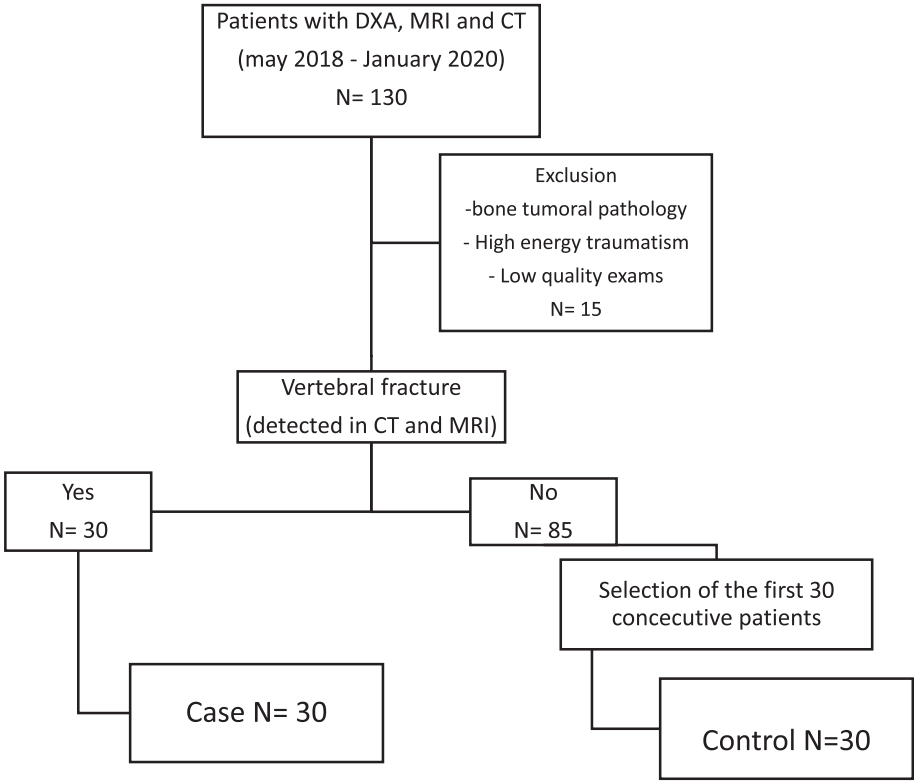

Fig. 1. Design and inclusion flow chart of the case-control study.

antenna was positioned on the top of the patient.

T1-weighted images [13,14] were recorded at 1.5 T (Philips® Ingenia) in the sagittal plane using a spin echo sequence (TR = 599 ms, TE = 8 ms, slice thickness = 4 mm, F0V = 325 × 325 × 66 mm). The total acquisition time was 3.5 min.

VOIs were selected as 4 mm thickness cylinders with a volume of 450 mm3 (Fig. 2).

Onto mid-sagittal image, a circular VOIs (1 cm^2) were positioned in the antero-superior edge of each vertebra (L1, L2, L3) by the two radiologists as recommended previously [15–17]. All fractured vertebras were excluded from the measurements.

2.3. CT scan acquisition and region of interest (ROI)

CT scans were recorded using a Lightspeed CT (General Electrics®) in both abdominal (120 kV. 550 mA) and lumbar (120 kV, 450 mA) regions. In both cases, slice thickness was 1.3 mm and slice interval was 1 and 0.6 mm respectively. Acquisition time was 4 and 10 s for the abdominal and lumbar protocol respectively. A daily calibration was performed.

We used a bone dedicated acquisition.

ROI was manually delineated by the two radiologists as an elliptic zone of 2 cm^2 in the anterior region of the vertebrae L1, L2 and L3, in the upper third, excluding cortical bone and the basivertebral vein. In the pathological group, the fractured vertebras (detected in both MRI and CT) were excluded from the measurements (Fig. 3).

Hounsfield Unit Bone density (HU BD) and texture parameters were quantified in axial sections as previously described [15].

Given the retrospective nature of the study, phantom calibration was not used.

2.4. DXA measurements

DXA measurements were performed using a Lunar iDXA™.

T-score, Z-score and aBMD were computed for the L1, L2, L3 vertebras and the corresponding values were averaged over the L1 to L3 region.

2.5. Texture analysis

First and second-order texture parameters were computed. First order parameters (Energy, Entropy, Mean and Median) are related to statistics computed from original images without considering the relationships among pixels. We computed Energy, Entropy, Mean and Median. Second order parameters refer to parameters which take into account relationships between pairs of pixels in the original image. We chose the Gray Level Co-occurrence Matrix (GLCM) [18–20] and Gray Level Run Length Matrix (GLRLM) [21–22].

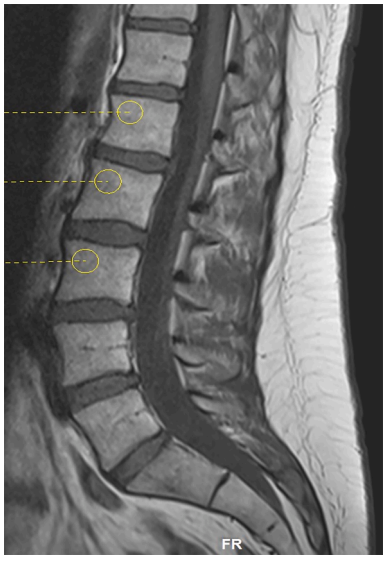

Fig. 2. MRI VOI on sagittal T1 acquisition.

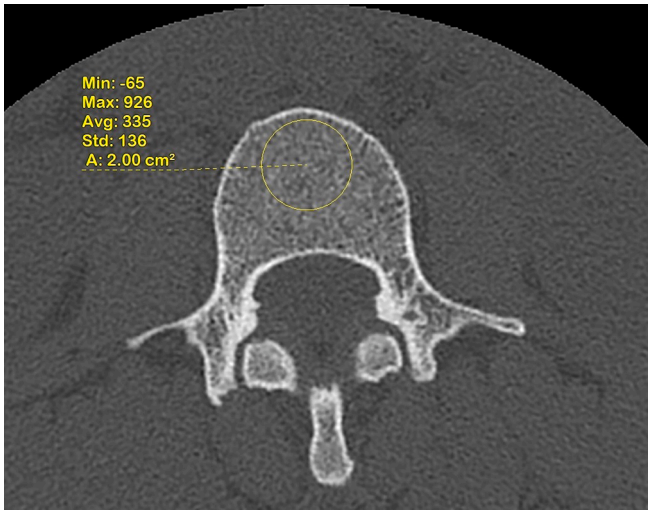

Fig. 3. CT ROI on axial section.

The GLCM matrix computes the combinations of pixel brightness values (grey levels) in an image. A GLCM of size Ng × Ng describes the second-order joint probability function of an image region constrained by the mask and is defined as P(i,j|δ,θ). The (i,j)th element of this matrix represents the number of times the combination of levels i and j occur in two pixels in the image, that are separated by a distance of δ pixels along angle θ. The distance δ from the center voxel is defined as the distance according to the infinity norm. For $\delta = 1$, this results in 2 neighbors for each of 13 angles in 3D (26-connectivity) and for $\delta = 2$ a 98-connectivity (49 unique angles). The GLCM analysis was performed to extract Contrast, Correlation (Corr), Joint Energy (JEnergy), Joint Entropy (JEntropy), Inverse difference moment (IDM), Maximum probability (MP), Sum average (SA) and Sum of squares (SOS) [18–20].

The GLRLM quantifies grey level runs defined as the number of consecutive pixels having the same grey level value. In a grey level run length matrix P(i,j|θ), the (i,j)th element describes the number of runs with grey level i and length j which occurs in the image (ROI) along an angle θ. We computed Short run emphasis (SRE), Long run emphasis (LRE), Grey level non uniformity (GLNU), Run length non uniformity (RLNU), Run percentage (RP), Low gray level run emphasis (LGLRE) and High grey level run emphasis (HGLRE) [21,22].

2.6. Statistical analyses

Measurements were obtained independently by 2 radiology research fellows (FP and PK) with both 5 years of experience. Comparisons of the two groups were performed using generalized linear model (with logit function) with subject as a random variable to take into account correlation of data (multiple measures per patient) within patients. We also performed ROC curve (receiver operating characteristic curve) to produce Area Under The Curve as a measure of performance of the feature to distinguish between the two groups. We also provided a threshold value of the feature associated with the Youden index maximum as with its linked sensitivity and specificity.

2.7. Decision tree

The subgroup of patients with osteoporotic fractures was also identified by a decision tree model based on the Classification And

Regression Tree method (CART). This method is a machine learning model, composed of hierarchical decision rules involving optimal cutoff values that recursively split independent factors into different groups. The CART algorithm was performed on the entire sample, without splitting into a train and a test sample, given of the low number of patients included in the study. It was based on the Gini impurity index using the Recursive Partitioning And Regression Trees (RPART) function. The method of "cost-complexity" pruning with a complexity parameter (α) equal to 0.01 was used in order to identify the most accurate tree and the optimal number of splits. This complexity parameter is a measure of how much additional accuracy a split must add to the entire tree to warrant additional complexity. The accuracy, sensitivity, and specificity of the CART model were calculated using the repeated K-Fold cross validation.

The most interesting parameters were initially identified by the Boruta package. Boruta is a feature selection algorithm which works as a wrapper algorithm around Random Forest. The Boruta package follows an all-relevant feature selection method and captures the whole set of features which are relevant to the outcome variable. As a second step, these parameters were introduced in the CART analysis to obtain the final decisional tree.

– Random Forest algorithm

Random forest analysis refers to the computation of multiple different decision trees built on random subsets of subjects with a final aim of classification. The computation of multiple decision trees provides a higher robustness to noise and a higher generalization as compared to a single decision tree [10,23].

– Measurements reproducibility

Both raters (FP and PK) computed texture parameters and CT Hounsfield Bone Density in a sample of 20 patients from group 1 and 20 patients from group 2. The intraclass correlation coefficients (ICC) were computed for each parameter using a two-way mixed method of absolute agreement. ICC values were ranked according to Koo and Li [24]. An ICC value<0.5 was considered as indicative of a poor reliability while an ICC value between 0.5 and 0.75 indicated a moderate reliability. Good and excellent reliability were related to ICC values between 0.75 and 0.9 and larger than 0.90 respectively [24,25].

Statistical analyses were performed using SPSS®.

3. Results

3.1. Groups description

G1 was composed of 23 women and 7 men and G2 of 22 women and 8 men. Patients from G1 (mean: 74.6 ± 12.1 years old, median: 79.5, Q1: 68, Q3: 83) were significantly older than those in G2 (mean: 56.1 ± 12.1 years old, median: 53.5, Q1: 47, Q3: 62). Among the 180 vertebrae analyzed, 42 were fractured (L1 = 16, L2 = 12, L3 = 14) and 12 patients had multiple fractures. The average percentage of collapse was 44 % (Genant grade 1, n = 10; Genant grade 2, n = 12; Genant grade 3, n = 19). In G1, 17 patients had no history of bone stock interest, 8 had inflammatory rheumatic diseases (4 of them were treated with long-term corticosteroids), 4 had an history of cancer without bone extension (2 breast cancers, 1 lung cancer, 1 vesical cancer) and 1 had a chronic obstructive pulmonary disease which needed long-term corticosteroids.

In G2, 8 patients had no history of bone stock interest, 21 had chronic rheumatic disease (1 of them was treated with long-term corticosteroids), 1 had a severe acute asthma requiring long-term corticosteroids, 1 had a chronic respiratory failure also requiring long-term corticosteroids.

CT acquisition protocols were heterogeneous in both groups. In G1, slice thickness was 0.6 mm for 20 subjects and 1.3 mm for the remaining 10. In G2, slice thickness was 0.6 mm for 13 subjects and 1.3 mm for 17 subjects. In G1, 4 patients did not have a reliable spinal DXA data on L1 due to interpositions, excessive collapse or arthrosis rearrangements that distorted the results. In G2, 4 patients did not have L1 consistent bone densitometry data for the same reasons.

The mean parameters values of the most relevant parameters for both groups together with the independent p values, the threshold with the best sensibility and specificity, and the Area Under the Curve (AUC) are summarized in Table 1 and Fig. 4. Maximum, Minimum and centiles values of all parameters are reported in table A. 1.

The inter observer reproducibility was good to excellent, with an intra-class correlation (ICC) between 0.90 and 0.98. Mean aBMD was similar in G1 (1.01 ± 0.23 g/cm^2) and G2 (1.03 ± 0.15 g/cm^2). T-score was also similar in G1 (-1.40) and G2 (-1.16).

On the contrary, twelve 1st and 2nd orders parameters differed significantly between the two groups ($p < 0.05$). More specifically, for CT images, Mean, Median and HGLRE were significantly different between the two groups. Regarding MR images, Contrast, Corr, Jentropy, JEnergy, IDM, LRE, GLNU, RP and LGLRE significantly differed between the groups.

Also, Hounsfield Unit Bone Density ($p < 0.001$) and Z-score ($p = 0.004$) were significantly different between the 2 groups.

3.2. R-PARt

Age and sex were systematically identified by the Boruta algorithm as indices of interest.

3.2.1. CT scan parameters

The Boruta algorithm identified Energy, Mean, Median, Sum Average, High Gray Level Run Emphasis, Hounsfield Unit Bone Density as the most interesting parameters for a decision tree (Fig. 5). Age and HU BD were selected by the RPART algorithm as the most relevant parameters for a decision tree (Fig. 6). The corresponding performance metrics were 82 % (accuracy), 73 % (sensibility), 86% (specificity), 76 % (positive predictable value) and 87 % (negative predictive value).

3.2.2. MRI parameters

The MRI texture parameters selected by Boruta were Joint Entropy, Joint Energy, Inverse Different Moment, Gray Level Non-Uniformity, Low Gray Level Run Emphasis. At this stage, the RPART algorithm identified age and Joint Entropy as the most relevant parameters for a decision tree (Fig. 7 and Fig. 8). The corresponding performance metrics were similar to those computed from the CT data i.e 82 % (accuracy), 73 % (sensitivity), 86 % (specificity), 80 % (positive predictable value) and 86 % (negative predictive value) (see Fig. 9)

3.3. Random Forest

The random Forest analysis computed using MRI texture parameters provided the following performance parameters: AUC = 0.909, Accuracy = 0.85 (0.79; 0.91), Sensitivity = 0.72 (0.55; 0.89), Specificity = 0.93 (0.86; 0.99), VPP = 0.85 (0.73; 0.97), VPN = 0.86 (0.78; 0.94).

When using CT-Scan texture parameters, the performance parameters were comparable AUC = 0.924, Accuracy = 0.89 (0.85; 0.92), Sensibility = 0.83 (0.67; 0.98), Specificity = 0.89 (0.76; 1.05), VPP = 0.80 (0.58; 1.01), VPN = 0.86 (0.76; 0.96).

4. Discussion

In this study we aimed at determining whether texture parameters computed from opportunistic CT and MRI could be used for the detection of vertebral fracture risk. We also intended to determine which parameters could be of most interest for a classification paradigm. We assessed 180 vertebrae of 60 patients divided in two groups: 30 patients had at least one vertebral fracture and in the control group 30 patients

Table 1
Mean, Standard Deviation (SD), P-value, threshold, sensibility (Se), specificity (Spe) and area under the curve (AUC) for the significant parameters in both groups.

Parameters	Imaging Modality	G1 = 30 Vertebrae = 48	G2 = 30 Vertebrae = 90	p value	Threshold	Se	Spe	AUC
Age		74.6 ± 12.1	56.1 ± 12.1	<0.0001	73.4	0.72	0.92	0.83
HU BD	CT	98.06 ± 31.49	148.4 ± 45.56	<0.0001	145.5	0.93	0.56	0.80
Median	CT	74.70 ± 59.26	135.2 ± 50.14	<0.0001	88.5	0.78	0.82	0.82
Mean	CT	78.11 ± 59.53	135.7 ± 49.20	<0.0001	92.9	0.83	0.79	0.81
GLNU	MRI	5.86 ± 3.17	8.91 ± 3.24	0.0003	5.8	0.65	0.86	0.79
Jentropy	MRI	7.88 ± 0.67	8.41 ± 0.50	0.0004	8.28	0.78	0.81	0.81
ZS	DXA	0.15 ± 1.71	−0.62 ± 1.11	0.0023	−0.65	0.37	0.90	0.65
Contrast	MRI	68.93 ± 44.87	45.88 ± 27.89	0.0062	46.04	0.67	0.66	0.67
Jenergy	MRI	0.01 ± 0.00	0.00 ± 0.00	0.0065	0.00	0.74	0.81	0.81
LGLRE	MRI	0.01 ± 0.01	0.01 ± 0.00	0.0110	0.01	0.78	0.61	0.73
IDM	MRI	0.16 ± 0.05	0.19 ± 0.04	0.0117	0.16	0.63	0.78	0.67
Corr	MRI	0.81 ± 0.11	0.86 ± 0.08	0.0179	0.79	0.41	0.91	0.63
HGLRE	CT	1015 ± 235.4	1120 ± 245.7	0.0239	1131.4	0.74	0.51	0.62
LRE	MRI	1.19 ± 0.10	1.25 ± 0.11	0.0348	1.16	0.50	0.90	0.68
RP	MRI	0.94 ± 0.02	0.93 ± 0.02	0.0373	0.95	0.52	0.84	0.67
Mean	MRI	951.7 ± 328.6	924.6 ± 397.2	0.7732	427.9	0.98	0.15	0.50

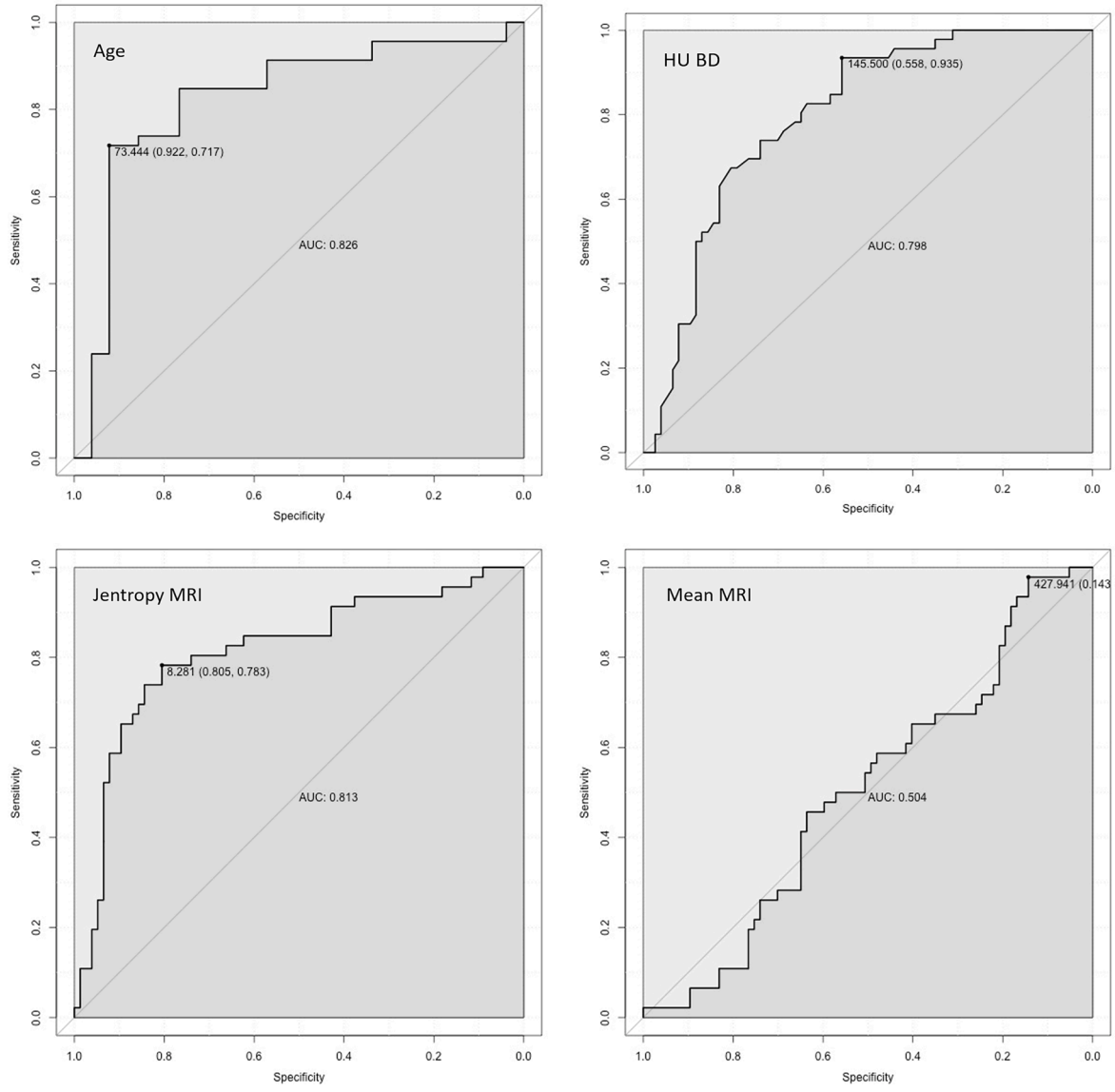

Fig. 4. ROC curves of the most relevant parameters used in the decision trees. (A) Age, (B) HU BD, (C) Jentropy-MRI, (D) Mean-MRI.

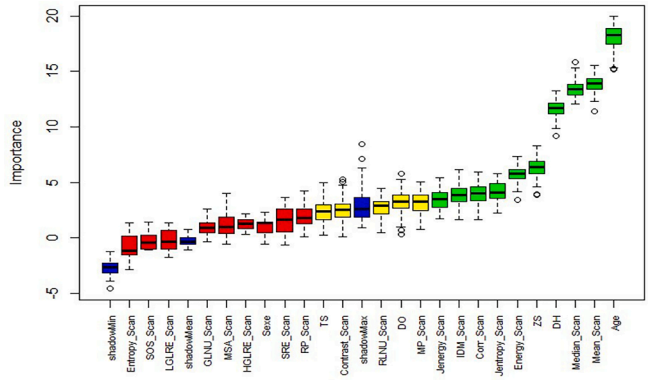

Fig. 5. CT Boruta package. Boruta package selecting the most relevant parameters obtained by CT-scan). 11 attributes confirmed important (in green): Age, Mean, Median, Correlation, Hounsfield density (HD), Energy, Inverse difference moment (IDM), Joint entropy, Z-Score, Maximum Probability (MP), Joint energy (Jentropy).

had no vertebral fracture. In the fractured group we had 30 % men which correspond to the prevalence of osteoporosis in men previously described [26,27].

We found that a significant number of 1st and 2nd orders texture parameters, four in CT and twelve in MRI, could discriminate subjects with a high risk of fragility vertebral fractures as compared to subjects with no vertebral fractures.

Surprisingly, T-score and aBMD were not able to distinguish the two groups. This reduced sensitivity had already been reported for DXA measurements. Bone fractures have been reported in 12.6 % to 17.9 % of subjects with a normal BMD [3] and a similar number of false negative subjects (14 %) has been reported for vertebral fractures [4]. Of interest, the rate of false negative subjects is much larger i.e. 47 % for mild vertebral fractures [4]. On the contrary, Z-score differed between the two groups and so likely as result of the significant age difference.

Of importance, the inter-rater reliability was good to excellent thereby indicating no bias related to manual measurements.

4.1. *Opportunistic CT*

Two first order texture parameters (Mean and Median) and one 2nd order parameters (HGLRE) were significantly different between the groups. Such a finding is in agreement with measurements reported previously in CT-scan [9]. Among the second order parameters, only one GLRM parameter (HGLRE) was found as of interest in the detection of vertebral fracture. A similar result has not been reported previously [9,28].

In opportunistic CT-scan, Hounsfield Unit Bone Density was significantly different between the groups ($p < 0.001$) and was identified as a parameter of high importance for patients' classification. The decision tree computed using the RPART algorithm showed that when patients were older than 73 the fracture risk was 85 %. In patients younger than 73, a HU BD larger than 120 HU was indicative of a very low risk (0.04 %) of fracture.

A similar threshold has been previously reported by Fang *et al.* who showed that a 150 HU threshold for a single measurement in L5 provided a 70 % sensitivity and 77 % specificity [15]. For a larger threshold i.e. 180 HU for measurements in L4, it rose respectively to 90 % and 43 % [15].

Using a Random Forest analysis including age, aBMD, HU BD and texture parameters, a very high AUC (0.924) was obtained and the corresponding sensitivity and specificity were 0.83 and 0.89 respectively. This value is larger than the AUC (0.88) reported by Valentinitsh *et al* who calculated vBMD and 3D texture features of the complete vertebral body [10] and also larger than the AUC value provided by the

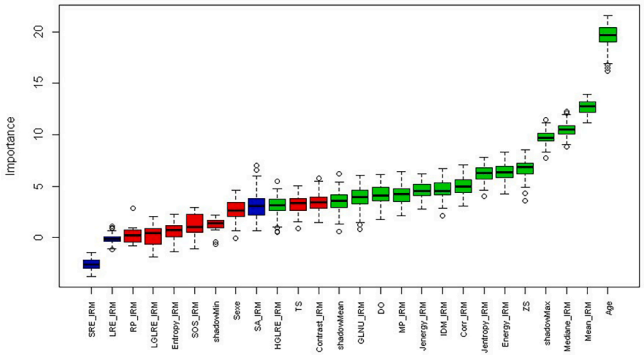

Fig. 7. MRI Boruta package. Boruta package selecting the most revelant parameters obtained by MRI (in green). 13 attributes confirmed important: Age, Mean, Median, Z-score (ZS), Energy, Joint Entropy (Jentropy), Correlation (Corr), Inverse difference moment (IDM), Joint energy (Jentropy), Maximum Probability (MP), Bone mineral density (BMD), Gray level non uniformity (GLNU), Heigh Gray Level Run Emphasis (HGLRE).

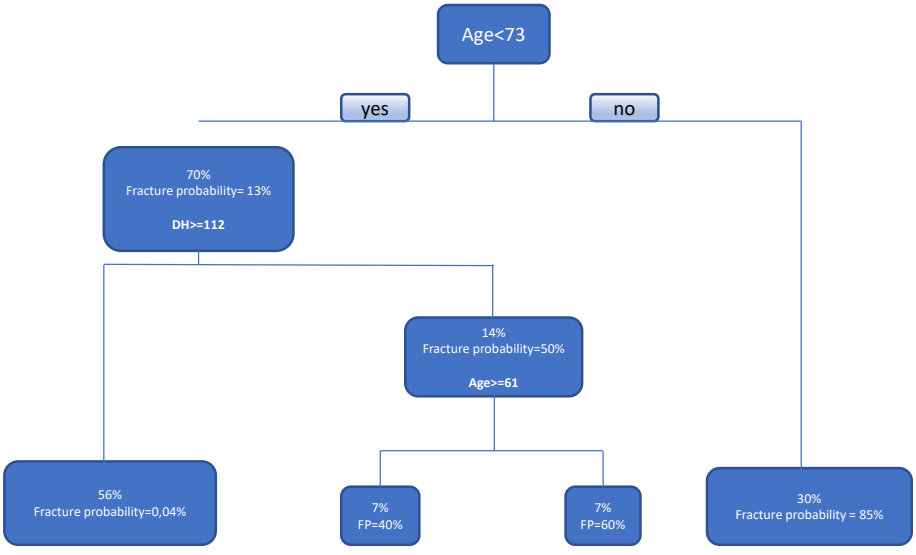

Fig. 6. CT decision tree. Probability to have a fracture (fracture probability: FP) according to age and Hounsfield Bone Density on opportunistic CT-scan.

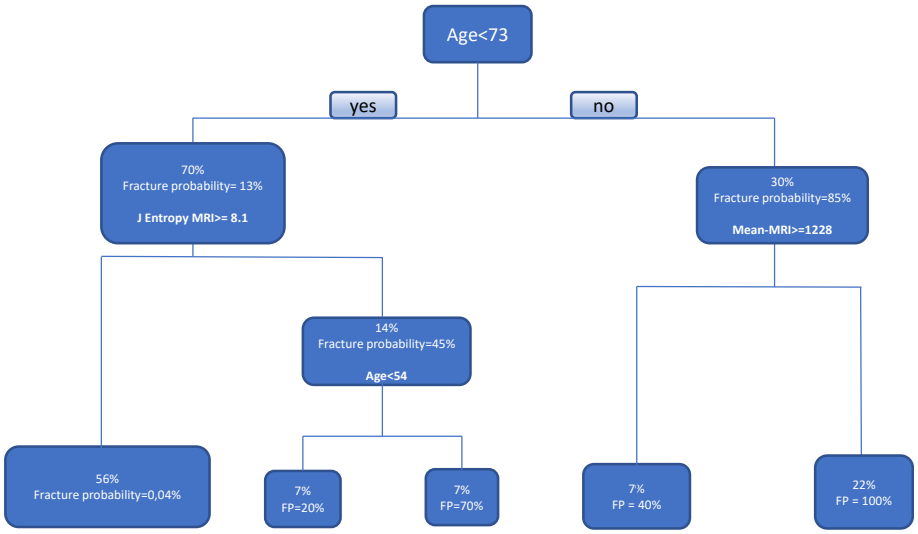

Fig. 8. MRI decision tree. Probability to have a fracture (fracture probability: FP) according to age, Joint Entropy and mean-MRI.

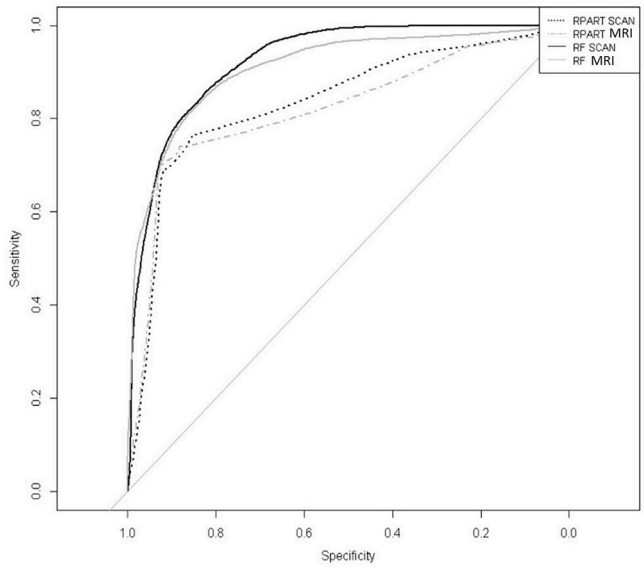

Fig. 9. ROC curves comparing Random Forest and RPART. Results in MRI and CT-Scan.

RPART analysis thereby reinforcing the idea that combining multiple parameters can be beneficial for the fracture risk prediction.

4.2. Opportunistic MRI

Texture parameters were computed from lumbar sagittal T1-weigthed MR images offering a a good signal/noise ratio and a good visibility of trabecular bone. According to previous studies, we did not attempt to assess bone marrow but trabecular architecture [11,14,28].

Nine texture parameters were significantly different between the two groups. The decision tree of fracture risk prediction was computed using age, Joint Entropy, and Mean texture parameter. On that basis, the fracture risk was 100 % for a patient older than 73 and with a mean MRI lower than 1228. The corresponding risk was very low (0.04 %) if the patient was younger than 73 and the Joint entropy was higher than 8.1. Of interest, although mean MRI was not significantly different between the two groups, this parameter provided the largest sensitivity for detecting fracture risks.

Using Random Forest algorithm, the AUC computed with CT-scan parameters was 0.924 and it was slightly lower when the MRI parameters were used (0.909). The corresponding sensitivity was 72 % and the specificity was 93 % thereby indicating that opportunistic MRI texture analysis is of interest for the detection of patients at risk of fragility fracture, even if the sensitivity is lower than the value obtained with CT. The lower sensitivity might be explained by the thinner slice thickness for CT (1.3 mm) as compared to MR images (4 mm).

The superiority of the Random Forest algorithm for the detection of patients with a high risk of fractures is in agreement with the study of Parmar *et al.* indicating that Random Forest analysis provided a higher predictive performance than decision tree [11]. Overall, texture analysis of opportunistic CT and MR images could be very sensitive to the detection of risk fracture when combined to machine learning algorithms.

Several limitations have to be acknowledged for the present study. In this preliminary study, the cohort of 60 patients might appear as small and the inclusion of additional subjects could be expected to be linked to a higher potential of fracture risk prediction. The age difference between the two groups was identified as a very important factor for the fracture risk detection. This difference can be explained by the late occurrence of vertebral osteoporotic fractures and the lack of associated pain.

This preliminary study is the very first to compare texture indices computed from on opportunistic CT and MR images. The corresponding results clearly indicate that age, HU-BD together with selected texture parameters could be used to assess risk fracture with a high sensitivity and specificity. The potential of fracture risk prediction might be enhanced with additional indices such as Z-scores and clinical risk factors [29]. Machine learning could be combined to deep learning approaches so as to provide a sensitive and specific tool of fracture risk prediction without additional examinations, radiation, patient's, and physician's time.

Funding

This research did not receive any specific grant from funding agencies in the public, commercial, or not-for-profit sectors.

Declaration of Competing Interest

The authors declare that they have no known competing financial interests or personal relationships that could have appeared to influence the work reported in this paper.

Acknowledgements

The author acknowledges Aix-Marseille University and Assistance Publique Hopitaux de Marseille.

References

[1] F. Borgström, L. Karlsson, G. Ortsäter, N. Norton, P. Halbout, C. Cooper, M. Lorentzon, E.V. McCloskey, N.C. Harvey, M.K. Javaid, J.A. Kanis, International Osteoporosis Foundation. Fragility fractures in Europe: burden, management and opportunities, Arch. Osteoporos. 15 (1) (2020) 59, https://doi.org/10.1007/s11657-020-0706-y.

[2] S.R. Cummings, L.J. Melton, Epidemiology and outcomes of osteoporotic fractures, The Lancet 359 (9319) (2002) 1761–1767, https://doi.org/10.1016/S0140-6736(02)08657-9.

[3] S.C.E. Schuit, M. Van Der Klift, A.E.A.M. Weel, C.E.D.H. de Laet, H. Burger, E. Seeman, A. Hofman, A.G. Uitterlinden, J.P. van Leeuwen, H.A. Pols, Fracture incidence and association with bone mineral density in elderly men and women: the Rotterdam Study, Bone 34 (1) (2004) 195–202, https://doi.org/10.1016/j.bone.2003.10.001.

[4] P.L. Jager, S. Jonkman, W. Koolhaas, A. Stiekema, B.H.R. Wolffenbuttel, R.H.J. A. Slart, Combined vertebral fracture assessment and bone mineral density measurement: a new standard in the diagnosis of osteoporosis in academic populations, Osteoporos. Int. 22 (4) (2011) 1059–1068, https://doi.org/10.1007/s00198-010-1293-3.

[5] C.H. Turner, S.C. Cowin, J.Y. Rho, R.B. Ashman, J.C. Rice, The fabric dependence of the orthotropic elastic constants of cancellous bone, J. Biomech. 23 (6) (1990) 549–561, https://doi.org/10.1016/0021-9290(90)90048-8.

[6] K. Engelke, Quantitative Computed Tomography-Current Status and New Developments, J. Clin. Densitom. 20 (3) (2017) 309–321, https://doi.org/10.1016/j.jocd.2017.06.017.

[7] L.J. Melton, B.L. Riggs, T.M. Keaveny, S.J. Achenbach, D. Kopperdahl, J.J. Camp, P.A. Rouleau, S. Amin, E.J. Atkinson, R.A. Robb, T.M. Therneau, S. Khosla, Relation of vertebral deformities to bone density, structure, and strength, J. Bone Miner. Res. 25 (2010) 1922–1930, https://doi.org/10.1002/jbmr.150.

[8] M.G. Lubner, A.D. Smith, K. Sandrasegaran, D.V. Sahani, P.J. Pickhardt, CT Texture Analysis: Definitions, Applications, Biologic Correlates, and Challenges, Radiographics 37 (5) (2017) 1483–1503, https://doi.org/10.1148/rg.2017170056.

[9] U.J. Muehlematter, M. Mannil, A.S. Becker, K.N. Vokinger, T. Finkenstaedt, G. Osterhoff, M.A. Fischer, R. Guggenberger, Vertebral body insufficiency fractures: detection of vertebrae at risk on standard CT images using texture analysis and machine learning, Eur. Radiol. 29 (5) (2019) 2207–2217, https://doi.org/10.1007/s00330-018-5846-8.

[10] A. Valentinitsch, S. Trebeschi, J. Kaesmacher, C. Lorenz, M.T. Löffler, C. Zimmer, T. Baum, J.S. Kirschke, Opportunistic osteoporosis screening in multi-detector CT images via local classification of textures, Osteoporos. Int. 30 (6) (2019) 1275–1285, https://doi.org/10.1007/s00198-019-04910-1.

[11] C. Parmar, P. Grossmann, J. Bussink, P. Lambin, H.J.W.L. Aerts, Machine Learning methods for Quantitative Radiomic Biomarkers, Sci. Rep. 5 (2015) 13087, https://doi.org/10.1038/srep13087.

[12] J.E. Burns, J. Yao, R.M. Summers, Vertebral Body Compression Fractures and Bone Density: Automated Detection and Classification on CT Images, Radiology 284 (3) (2017) 788–797, https://doi.org/10.1148/radiol.2017162100.

[13] J. Marques, H.K. Genant, M. Lillholm, E.B. Dam, Diagnosis of osteoarthritis and prognosis of tibial cartilage loss by quantification of tibia trabecular bone from MRI, Magn. Reson. Med. 70 (2) (2013) 568–575, https://doi.org/10.1002/mrm.24477.

[14] J.W. MacKay, P.J. Murray, B. Kasmai, G. Johnson, S.T. Donell, A.P. Toms, Subchondral bone in osteoarthritis: association between MRI texture analysis and histomorphometry, Osteoarthritis Cartilage 25 (5) (2017) 700–707, https://doi.org/10.1016/j.joca.2016.12.011.

[15] J. Fang, A. Franconeri, J. Boos, J. Nimhuircheartaigh, Z. Zhang, A. Brook, O. R. Brook, Opportunistic Bone Density Measurement on Abdomen and Pelvis Computed Tomography to Predict Fracture Risk in Women Aged 50 to 64 Years Without Osteoporosis Risk Factors, J. Comput. Assist. Tomogr. 42 (5) (2018) 798–806, https://doi.org/10.1097/RCT.0000000000000744.

[16] X. Banse, J.P. Devogelaer, E. Munting, C. Delloye, O. Cornu, M. Grynpas, Inhomogeneity of human vertebral cancellous bone: systematic density and structure patterns inside the vertebral body, Bone 28 (5) (2001) 563–571, https://doi.org/10.1016/S8756-3282(01)00425-2.

[17] R. Eastell, S.L. Cedel, H.W. Wahner, B.L. Riggs, L.J. Melton, Classification of vertebral fractures, J. Bone Miner. Res. 6 (3) (1991) 207–215, https://doi.org/10.1002/jbmr.5650060302.

[18] P. Ranjanomennahary, S.S. Ghalila, D. Malouche, A. Marchadier, M. Rachidi, C. Benhamou, C. Chapard, Comparison of radiograph-based texture analysis and bone mineral density with three-dimensional microarchitecture of trabecular bone, Med. Phys. 38 (2011) 420–428, https://doi.org/10.1118/1.3528125.

[19] S. Herlidou, R. Grebe, F. Grados, N. Leuyer, P. Fardellone, M.E. Meyer, Influence of age and osteoporosis on calcaneus trabecular bone structure: A preliminary in vivo MRI study by quantitative texture analysis, Magn. Reson. Imaging 22 (2004) 237–243, https://doi.org/10.1016/j.mri.2003.07.007.

[20] J. Thevenot, J. Hirvasniemi, P. Pulkkinen, M. Määttä, R. Korpelainen, S. Saarakkala, T. Jämsä, Assessment of Risk of Femoral Neck Fracture with Radiographic Texture Parameters: A Retrospective Study, Radiology 272 (2014) 184–191, https://doi.org/10.1148/radiol.14131390.

[21] R. Karunanithi, S. Ganesan, T.M.R. Panicker, M.P. Korath, K. Jagadeesan, Assessment of bone mineral density by DXA and the trabecular microarchitecture of the calcaneum by texture analysis in pre- and postmenopausal women in the evaluation of osteoporosis, J. Med. Phys. 32 (2007) 161–168, https://doi.org/10.4103/0971-6203.37481.

[22] E. Lespessailles, C. Gadois, I. Kousignian, J.P. Neveu, P. Fardellone, S. Kolta, C. Roux, J.P. Do-Huu, C.L. Benhamou, Clinical interest of bone texture analysis in osteoporosis: A case control multicenter study, Osteoporos. Int. 19 (2008) 1019–1028, https://doi.org/10.1007/s00198-007-0532-8.

[23] S. Rastegar, M. Vaziri, Y. Qasempour, M.R. Akhash, N. Abdalvand, I. Shiri, H. Abdollahi, H. Zaidi, Radiomics for classification of bone mineral loss: A machine learning study, Diagn. Interv. Imaging. 101 (9) (2020) 599–610, https://doi.org/10.1016/j.diii.2020.01.008.

[24] T.K. Koo, M.Y. Li, A Guideline of Selecting and Reporting Intraclass Correlation Coefficients for Reliability Research, J. Chiropr. Med. 15 (2) (2016) 155–163, https://doi.org/10.1016/j.jcm.2016.02.012.

[25] M. Benchoufi, E. Matzner-Lober, N. Molinari, A.S. Jannot, P. Soyer, Interobserver agreement issues in radiology, Diagn. Interv. Imaging 101 (10) (2020) 639–641, https://doi.org/10.1016/j.diii.2020.09.001.

[26] J. Lee, S. Lee, S. Jang, O.H. Ryu, Age-Related Changes in the Prevalence of Osteoporosis according to Gender and Skeletal Site: The Korea National Health and Nutrition Examination Survey 2008–2010, Endocrinol. Metab. 28 (3) (2013) 180–191, https://doi.org/10.3803/EnM.2013.28.3.180.

[27] N. Salari, H. Ghasemi, L. Mohammadi, M.H. Behzadi, E. Rabieenia, S. Shohaimi, M. Mohammadi, The global prevalence of osteoporosis in the world: a comprehensive systematic review and meta-analysis, J. Orthop. Surg. Res. 16 (1) (2021) 609. https ://doi.org/10.1186/s13018-021-02772-0.

[28] N. Sollmann, E.A. Becherucci, C. Boehm, M.E. Husseini, S. Ruschke, E. Burian, J. S. Kirschke, T. Link, K. Subburaj, D.C. Karampinos, R. Krug, T. Baum, M. Dieckmeyer, Texture Analysis Using CT and Chemical Shift Encoding-Based Water-Fat MRI Can Improve Differentiation Between Patients With and Without Osteoporotic Vertebral Fractures, Front. Endocrinol. 12 (2022), 778537, https://doi.org/10.3389/fendo.2021.778537.

[29] X. Wang, A. Sanyal, P.M. Cawthon, L. Palermo, M. Jekir, J. Christensen, K. E. Ensrud, S.R. Cummings, E. Orwoll, D.M. Black, T.M. Keaveny, Prediction of new clinical vertebral fractures in elderly men using finite element analysis of CT scans, J. Bone Miner. Res. 27 (4) (2012) 808–816, https://doi.org/10.1002/jbmr.1539.